Available online at www.sciencedirect.com

ScienceDirect

Ceramics International 40 (2014) 2663–2668

CERAMICS INTERNATIONAL

www.elsevier.com/locate/ceramint

Synthesis and luminescence properties of $Y_2O_2S:Dy^{3+}$, Mg^{2+}, Ti^{4+} phosphors prepared by sol–gel process

Ping Huang[a], Xueqin He[a], Cai'e Cui[a,b,*], Lei Wang[a]

[a]Physics and Optoelectronic Engineering College, Taiyuan University of Technology, Taiyuan 030024, China
[b]Observation and Control Technology Research Institute, Taiyuan University of Technology,Taiyuan 030024,China

Received 15 August 2013; received in revised form 1 October 2013; accepted 14 October 2013
Available online 22 October 2013

Abstract

$Y_2O_2S:Dy^{3+}$, Mg^{2+}, Ti^{4+} white-light long-lasting phosphors were synthesized by sol–gel method. $Y_2O_2S:Dy^{3+}$, Mg^{2+}, Ti^{4+} phosphors were characterized by X-ray diffraction, photoluminescence spectroscopy and thermally stimulated spectrometry. The results showed that the samples calcined at different temperatures from 900 °C to 1200 °C were composed of the pure Y_2O_2S phase. Under 359 nm UV excitation, the phosphor presented white luminescence due to mixing of the dominating emissions centered at 488 nm (blue) and 579 nm (yellow), corresponding to $^4F_{9/2}\rightarrow{}^6H_{15/2}$ and $^4F_{9/2}\rightarrow{}^6H_{13/2}$ transitions of Dy^{3+}, respectively. Both the fluorescence intensity and afterglow time reached the largest values in the phosphor calcined at 1200 °C and the afterglow time could last for over 65 min (≥ 1 mcd/m^2) when the excited source was cut off.

Keywords: White-light long-lasting phosphor; Yttrium oxysulfide; Luminescence; Sol–gel method

1. Introduction

The long afterglow materials have great potentials in applications such as luminous paints, emergency lighting, safe traffic, wall painting, films, artificial fibers, rubbers textiles ceramics and biomedical nanodevices [1–4]. From the point of practical application, a white afterglow phosphor is most suitable as illuminating light source. Therefore, the white-light long-lasting phosphors with high luminescence efficiency and good chemical stability are badly needed.

The phosphor doped with Dy^{3+} is an excellent candidate for white-light phosphors because the white color can be obtained by the appropriate mixing of the two main emissions $^4F_{9/2}\rightarrow{}^6H_{15/2}$ (blue) and $^4F_{9/2}\rightarrow{}^6H_{13/2}$ (yellow) of Dy^{3+} [5]. There are many hosts that can be activated by Dy^{3+} ions, such as borates ($Ba_2LiB_5O_{10}:Dy^{3+}$) [6], aluminates ($Sr_3Al_2O_6:Eu^{2+}$, Dy^{3+}) [7], silicates ($Ca_xMgSi_2O_{5+x}:Dy^{3+}$) [8], vanadates ($YVO_4:Dy^{3+}$) [9], phosphates ($YPO_4:Ce^{3+}$, Dy^{3+}) [10], oxides ($Y_2O_3:Dy^{3+}$) [11], and some oxysulfides ($Y_2O_2S:Dy^{3+}$, Mg^{2+}, Si^{4+}) [12]. Of all the hosts, yttrium oxysulfide has been attracted much attention due to its stable crystal structure and high thermal stability [13]. Thus, $Y_2O_2S:Dy^{3+}$ phosphor may be an excellent material for the development of white-light long-lasting phosphor. In addition, the Dy^{3+} doped yttrium oxysulfide phosphors have already been synthesized by our research group using solid-state reaction [12]. However, this synthesis method often need some additives as flux to obtain a single phase, resulting in inhomogeneous products with broad particle size distribution and low surface area. Compared with the solid-state reaction method, sol–gel process has some advantages, including easy stoichiometric control, good homogeneity and the final product possessing smaller particle size and better distribution.

To our knowledge, no studies on $Y_2O_2S:Dy^{3+}$, Mg^{2+}, Ti^{4+} phosphors prepared by sol–gel method, have ever been reported. In this paper, $Y_2O_2S:Dy^{3+}$, Mg^{2+}, Ti^{4+} white-light long-lasting powders were prepared via sol–gel method, and

*Corresponding author at: Physics and Optoelectronic Engineering College, Taiyuan University of Technology, Taiyuan 030024, China.
Tel.: +86 035 1417 5345.
E-mail address: tytgcejy@sina.com (C. Cui).

0272-8842/$ - see front matter © 2013 Elsevier Ltd and Techna Group S.r.l. All rights reserved.
http://dx.doi.org/10.1016/j.ceramint.2013.10.058

the luminescence properties of the obtained powders were investigated.

2. Experimental

Y_2O_3 (3N), Dy_2O_3 (4N) and $Mg(OH)_2 \cdot 4MgCO_3 \cdot 6H_2O$ (AR) were used as the starting materials in the sol–gel route. The mixed solution of metal nitrates with nominal atomic ratios Y:Dy:Mg = 2:0.01:0.06 was obtained by dissolving Mg $(OH)_2 \cdot 4MgCO_3 \cdot 6H_2O$, Y_2O_3 and Dy_2O_3 in dilute nitric acid. Then ammonia solution of EDTA with molar ratio of total metal cations to EDTA 1:1.1 was gained by dissolving EDTA in ammonia. The above two solutions were mixed and stirred at 80 °C for 1 h. Then butyl titanate with nominal atomic ratios Y:Ti = 2:0.06 was added to the above solution. Then the PH was adjusted at about 4 using aqua ammonia. By keeping the solution at 80 °C for 5 h under constant stirring, the solution became viscous. After the wet gel was dried at 80 °C for 7 h, white dried-gels were obtained. Then the dried-gels were calcined at 600 °C for 2 h in air atmosphere. Finally, the $Y_2O_2S:Dy^{3+}$, Mg^{2+}, Ti^{4+} phosphors were obtained by sintering precursors in a weak reductive atmosphere of CS_2 at different temperatures (900–1300 °C) for 2 h. The heating rate was 6 °C/min.

The crystal structure of the products was examined by SHIMADZU-6000 X-ray generator with Cu Kα ($\lambda = 0.15406$ nm) radiation and the scan step was 0.02°. The photoluminescence (PL) spectra of the samples was measured by an F-280 spectrophotometer with a 150W Xe lamp as the excitation source. The afterglow properties were collected using the brightness meter (ST-86LA) with the help of a stopwatch. The thermoluminescence (TL) curves were obtained on a model FJ-427A1TL meter with a heating rate of 1 K/s from room temperature to 673 K. The samples were excited for 10 min by 254 nm UV radiation standard lamp with a power of 6W before measuring their TL curves and the afterglow decay curves. All measurements were carried out at room temperature except for the TL curves.

3. Results and discussion

3.1. Phase characterization

Fig. 1 shows the XRD patterns of the samples calcined at different temperatures for 2 h in a weak reductive atmosphere of CS_2. It indicates that the samples at calcination temperatures varying from 900 °C to 1200 °C are composed of pure Y_2O_2S phase which accords with JCPDS card no. 24-1424. The intensity of the Y_2O_2S diffraction peaks increases with the increase of calcination temperature, which indicates that the crystallinity of the sample becomes better. When the temperature reaches 1200 °C, the XRD pattern of sample becomes the strongest. Above 1200 °C, the powder becomes a mixture of cubic Y_2O_3 crystalline phase and hexagonal Y_2O_2S crystalline phase. The reason may be that the Y_2O_2S break up into Y_2O_3.

3.2. Photoluminescence spectra and CIE chromaticity coordinate of $Y_2O_2S:Dy^{3+}$, Mg^{2+}, Ti^{4+} phosphors

The excitation spectra of $Y_2O_2S:Dy^{3+}$, Mg^{2+}, Ti^{4+} phosphors at different calcination temperatures is shown in Fig. 2. The excitation spectra of five samples is composed of a broad band with a peak at 267 nm which is attributed to the absorption between bands of the Y_2O_2S host lattice, and some narrow peaks at 332, 359, 372, 392 nm, originated from the ground state $^6H_{15/2}$ to the excitation states of $^6P_{3/2}$, $^6P_{7/2}$, $^6P_{5/2}$ and $^4I_{13/2}$, respectively [14]. The peak intensity enhances with increasing calcination temperatures from 900 °C to 1200 °C. The intensity of the sample is the strongest when heat-treated at 1200 °C. The intensity of excitation spectra starts to decrease when the temperature exceeds this critical value. The result also indicates that the absorption peak shifts to the blue (from from 267 to 261 nm) as the temperature decreases. This may be associated with the quantum size effect of the

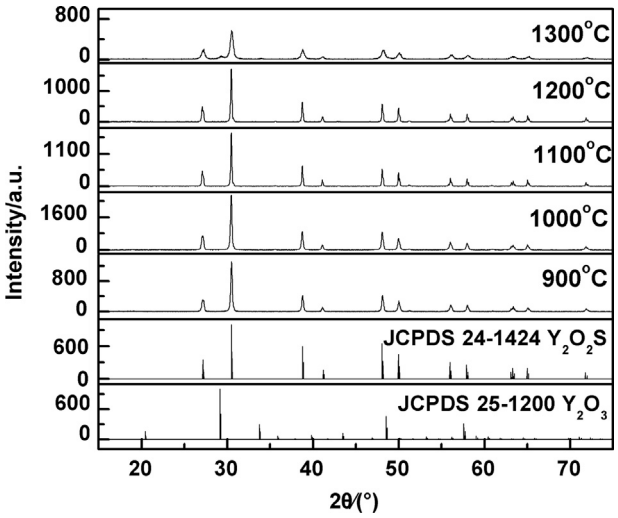

Fig. 1. The XRD patterns of $Y_2O_2S:Dy^{3+}$, Mg^{2+}, Ti^{4+} calcined at different temperatures.

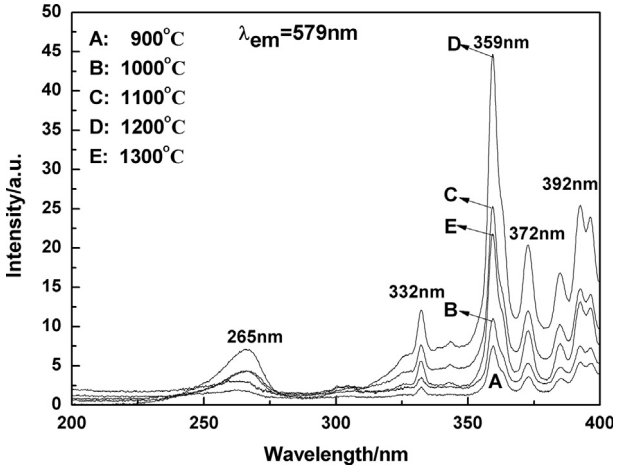

Fig. 2. The excitation spectra of $Y_2O_2S:Dy^{3+}$, Mg^{2+}, Ti^{4+} calcined at different temperatures.

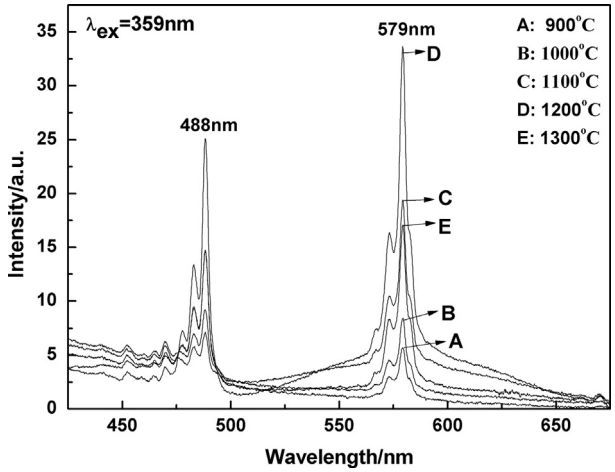

Fig. 3. The emission spectra of $Y_2O_2S:Dy^{3+}$, Mg^{2+}, Ti^{4+} calcined at different temperatures.

nanometer phosphor, which increased the energy of the electrons and resulted in a larger band gap, and thus required higher energy to excite the luminescent powders.

Fig. 3 displays the emission spectra of $Y_2O_2S:Dy^{3+}$, Mg^{2+}, Ti^{4+} phosphors at different calcination temperatures excited by 359 nm UV light. All of the emissions observed are due to the 4f→4f transitions of Dy^{3+}. The emission peaks at 488 nm (blue emission) and 579 nm (yellow emission) are assigned to the $^4F_{9/2}\rightarrow{}^6H_{15/2}$ and $^4F_{9/2}\rightarrow{}^6H_{13/2}$ transition of Dy^{3+} respectively. The blue emission is the nature of magnetic dipole transition, and the yellow emission belongs to the hypersensitive (forced electric dipole) transition following the selection rule, $\Delta J=2$. In the studied $Y_2O_2S:Dy^{3+}$, Mg^{2+}, Ti^{4+} phosphors, the intensity of yellow emission is greater than that of the blue emission. It is well known that the hypersensitive transition is strongly influenced by the outside environment surrounding Dy^{3+}, while the magnetic dipole transition is not. When the Dy^{3+} is located at a low symmetry site (without inversion symmetry), the yellow emission would be stronger than the blue ones; whereas, the blue emission is dominant in the emission spectrum [15,16]. Thus, the stronger yellow emission indicates that Dy^{3+} ions take the site without inversion symmetry. In addition, it can also be found that with the increase in the calcining temperature from 900 °C to 1200 °C, the intensity of emission peaks is increased and reaches a maximum at 1200 °C. One can also find that the emission lines are broadened somewhat because there are several Stark levels for the $^4F_{9/2}$ and ^6H_J [17].

The CIE chromaticity coordinate of $Y_2O_2S:Dy^{3+}$, Mg^{2+}, Ti^{4+} phosphors calcined at different temperatures is shown in Fig. 4. The CIE chromaticity coordinates of samples can be obtained by the emission spectra data. They vary from (0.21, 0.19), (0.25, 0.23), (0.33, 0.33), (0.38, 0.37) to (0.30,0.30) corresponding to points A, B, C, D, E. The chromaticity coordinates of samples gradually move to the warm white side and approach the yellow region with the increase in the calcining temperature from 900 °C to 1200 °C. It is because that the intensity of yellow emission is increased gradually with the increasing temperatures. This change is consistent with Fig. 3. In Fig. 4, point C is the closest to point W which delegates the ideal white.

In order to detect the white afterglow in the $Y_2O_2S:Dy^{3+}$, Mg^{2+}, Ti^{4+} phosphor, the afterglow decay curves and the afterglow emission spectra of the phosphor calcined under 1200 °C after the 254 nm UV radiation for 5 min are plotted in Fig. 5. The decay curves of 488 nm and 579 nm emissions are similar, indicating that the emissions have similar decay ratio. As shown in the inset picture of Fig. 5, we have measured the

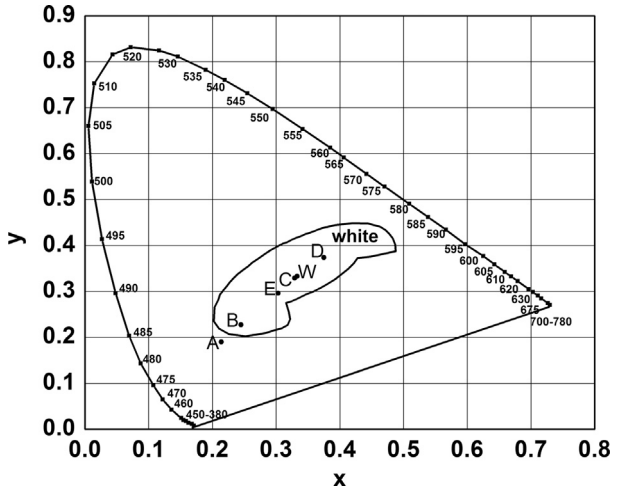

Fig. 4. The CIE chromaticity diagram of $Y_2O_2S:Dy^{3+}$, Mg^{2+}, Ti^{4+} phosphors calcined at different temperatures: (A) 900 °C; (B) 1000 °C; (C) 1100 °C; (D) 1200 °C; and (E) 1300 °C.

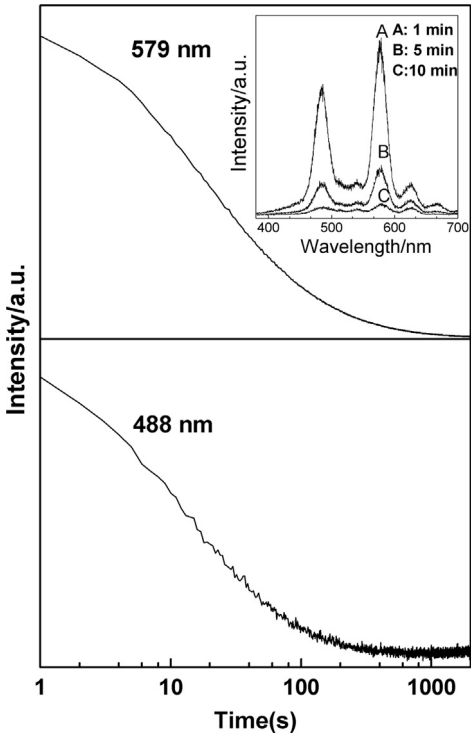

Fig. 5. The afterglow intensity decay curves of different emissions in $Y_2O_2S:Dy^{3+}$, Mg^{2+}, Ti^{4+} phosphor calcined at 1200 °C (the inset picture shows the afterglow emission spectra of the sample at different times after the removal of the excitation).

afterglow emission spectra of the sample at different times after switching off the excitation source. The afterglow emission spectra are observed in the same region as the emission spectra. The shape and the location of main emission spectra are found to be almost identical. Thereby, we can obtain white phosphorescence during the decay process.

3.3. Afterglow decay curves and TL curves of the samples

Fig. 6 shows the afterglow decay curves of the synthesized samples after irradiation with 254 nm for 10 min. The inset in Fig. 6 shows the initial intensity and afterglow time with different calcination temperatures. The decay behavior of $Y_2O_2S:Dy^{3+}$, Mg^{2+}, Ti^{4+} phosphor shows a rapid decay at the beginning and then a stable long persistent process. It is reported that the afterglow decay curve can be well fitted by an empirical formula [18]:

$$I = A_1\exp(-t/\tau_1)+A_2(-t/\tau_2) \quad (1)$$

where I is the phosphorescence intensity; A_1 and A_2 are constants; t is the time; τ_1 and τ_2 are the decay times for the exponential components, respectively. The long afterglow-decay fitting parameters are given in Table 1. As shown in Table 1, the values of τ_2 are bigger than those of τ_1, which reveal that the decay processes of these phosphors behave in terms of a double exponential decay model. At first it shows a rapid decay, and then a long-lasting phosphorescence.

The afterglow mechanism can be explained by the contribution from electron traps formed by the co-doped Mg^{2+} and Ti^{4+} ions. They occupy the same lattice sites as Y^{3+} do. To keep charge balance, $2Y^{3+}$ ions are replaced by $1Mg^{2+}$ and $1Ti^{4+}$ ion. However, such replacement breaks the charge balance around local lattice site and causes the formation of new electronic donating and accepting levels between the host lattice band gap, that is, an excessive positive charge which serves as the electron trap around the doped Ti^{4+} ion is created. One of the two kinds of ions absorbs energy and thermally transfers the excited electrons to the other kinds of ions which serves as trap centers. The trap of stored energy which is constituted by Mg^{2+} and Ti^{4+} ions serves as donor leveling and Dy^{3+} serves as acceptor leveling. The trapping of excited electrons and thermally released processes cause the appearance of afterglow [19].

It also be found in Fig. 6 that the initial brightness and afterglow time of the phosphor enhanced when increasing calcination temperatures from 900 °C to 1200 °C. The sample calcined at 1200 °C shows the optimal initial brightness and afterglow time, and the decay time can last for over 65 min (≥ 1 mcd/m^2). This can be attributed to the rapid diffusion of rare earths ions into the Y_2O_2S host lattice at relatively high temperature. But when the calcination temperature is too high (1300 °C), the luminescence properties of the powders were decreased.

It has generally been agreed that the initial intensity and afterglow time of the phosphors were affected greatly by the depth and the density of trap which was formed by the doped

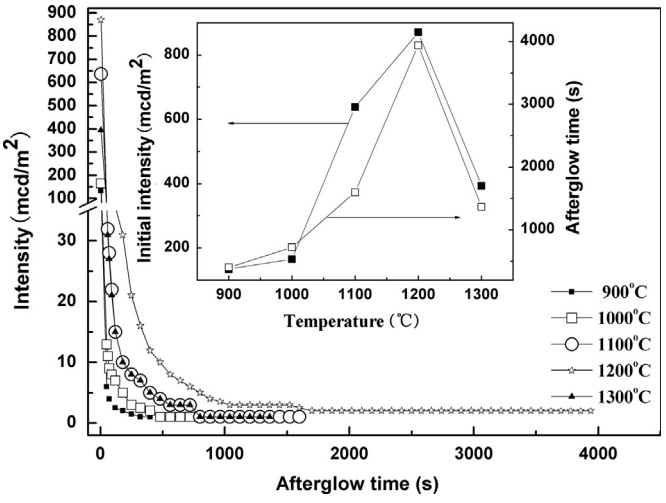

Fig. 6. The afterglow decay curves of $Y_2O_2S:Dy^{3+}$, Mg^{2+}, Ti^{4+} phosphors calcined at different temperatures, (the inset picture shows the initial intensity and afterglow time with different calcination temperatures).

Table 1
Fitting parameters of samples calcined at different temperatures.

Calcination temperatures (°C)	*Parameters*	
	τ_1	τ_2
900	1.08	8.89
1000	1.22	20.79
1100	3.14	64.99
1200	4.69	198.32
1300	2.33	63.48

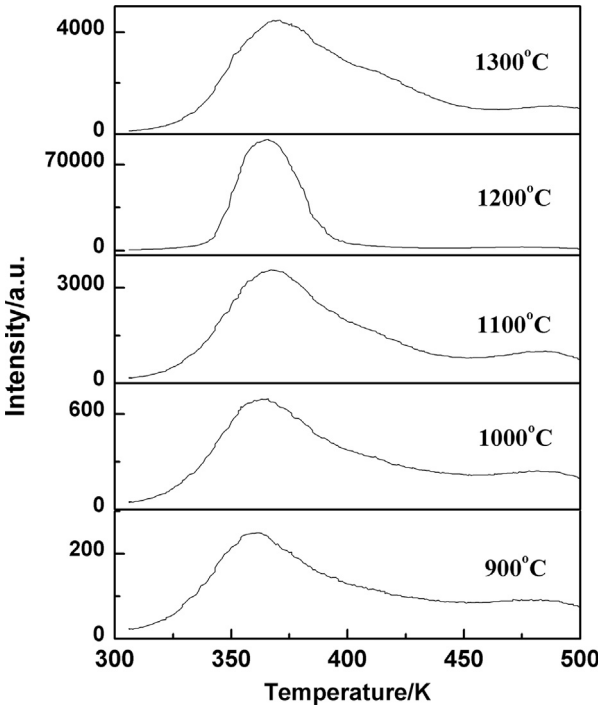

Fig. 7. The TL curves of $Y_2O_2S:Dy^{3+}$, Mg^{2+}, Ti^{4+} phosphors calcined at different temperatures.

Table 2
E values of samples with different calcination temperatures.

Temperature (°C)	T_m (K)	T_1 (K)	T_2 (K)	τ (K)	δ (K)	ω (K)	μ_g	c_τ	b_τ	E (eV)
900	362	336	402	26	40	66	0.61	2.08	2.38	0.75
1000	366	341	406	25	40	65	0.62	2.11	2.42	0.82
1100	367	344	406	23	39	62	0.63	2.14	2.46	0.93
1200	366	350	381	16	15	31	0.48	1.69	1.83	1.10
1300	371	346	416	25	45	70	0.64	2.17	2.50	0.87

ions [20]. So the TL curves of phosphors were measured and showed in Fig. 7. For all samples, the TL peaks are located in the region of 323–383 K which are helpful to produce the afterglow phenomenon [21]. With the increase of calcination temperatures from 900 °C to 1200 °C, the intensity of TL peak is increased gradually. The intensity of TL peak reaches maximum when the sample was calcined at 1200 °C. The following is Chen's equations for calculating the trap depth E [22]:

$$E = c_\tau k T_m^2/\tau - b_\tau 2kT_m \quad (2)$$

$$c_\tau = 1.51+3(\mu_g-0.42),\ \ b_\tau = 1.58+4.2(\mu_g-0.42) \quad (3)$$

$$\tau = T_m - T_1, \delta = T_2 - T_m, \omega = T_2 - T_1, \mu_g = \delta/\omega \quad (4)$$

where T_1, T_m and T_2 represent the temperature of half-intensity at low-temperature side, peak temperature, temperature of half-intensity at high-temperature side of TL peak, τ is the left half width, δ is the right half width, ω is the total half intensity width, k is Boltzmann's constant and μ_g is the symmetry factor. The trap parameters are estimated and listed in Table 2.

Defects with a suitable depth could capture the carrier more effectively and deliver them more slowly to the emission centers which result in long afterglow phenomenon [23]. If the trap level is too shallow, the electron in the trap can return to the energy level of excited state easily, thus resulting in short afterglow lifespan [24]. However, it will be difficult for trapped electrons to be released if the trap level is too deep. In the Table 2, the sample calcined at 1200 °C has the deepest trap depth (1.1 eV), and it shows the optimal initial luminance and afterglow time. When the calcination temperature exceeds 1200 °C, the trap depth of $Y_2O_2S:Dy^{3+}$, Mg^{2+}, Ti^{4+} phosphor can not be improved any more. From Table 2 and Fig. 7, for $Y_2O_2S:Dy^{3+}$, Mg^{2+}, Ti^{4+} phosphor, the high trap density and deep depth are suitable to produce optimal afterglow time. This is because that the materials have a deeper depth of traps, a large amount of electrons can be captured and be harder to release from traps to combine with holes under the action of thermal disturbances, the afterglow time will last much longer.

4. Conclusions

$Y_2O_2S:Dy^{3+}$, Mg^{2+}, Ti^{4+} white-light long-lasting phosphors were prepared via sol gel method in a weak reductive atmosphere of CS_2. With XRD data, the phosphor was characterized to be single phase Y_2O_2S after being calcined at temperatures from 900 °C to 1200 °C. The absorption peak of excitation spectra shifts to the blue as the temperature decreases. Under 359 nm UV irradiation, the white-light could be obtained by the appropriate mixing of blue emission and yellow emission from the transitions between 4f levels of Dy^{3+}. When calcined at 1200 °C, the sample shows the optimal afterglow properties, and the decay time can last for over 65 min (≥ 1 mcd/m^2).

Acknowledgments

This present work was financially supported by the National Natural Science Foundation of China (No. 51072128), the Key Research Project of Science and Technology of Shanxi (No. 2011 0321040-01) and the Program for the Top Young Academic Leaders of Higher Learning Institutions of Shanxi.

References

[1] B.F. Lei, Y.L. Liu, J.W. Zhang, J.X. Meng, S.Q. Man, S.Z. Tan, Persistent luminescence in rare earth ion-doped gadolinium oxysulfide phosphors, J. Alloys Compd. 495 (2010) 247–253.
[2] J.W. Zhang, Y.L liu, S.M. Man, Afterglow phenomenon in erbium and titanium co-doped Gd_2O_2S phosphors, J. Lumin. 117 (2006) 141–146.
[3] L. Zhang, Z. Lu, H. Yang, P.D. Han, N.C. Xu, Q.T. Zhang, Preparation of Dy^{3+} activated strontium orthosilicate ($Sr_2SiO_4:Dy^{3+}$) phosphors and its photoluminescent properties, J. Alloys Compd. 512 (2012) 5–11.
[4] Thomas Maldiney, BrunoViana, Aurélie Bessière, Didier Gourier, Michel Bessodes, Daniel Scherman, Cyrille Richard, In vivo imaging with persistent luminescence silicate-based nanoparticles, Opt. Mater. 35 (2013) 1852–1858.
[5] X.H. Zhang, Z.M. Lu, F.B. Meng, L. Hu, X.W. Xu, J. Lin, Luminescence properties of $Ca_3Si_2O_7:Dy^{3+}$ phosphor for white light-emitting diodes, Mater. Lett. 79 (2012) 292–295.
[6] Y.F. Liu, Z.P. Yang, Q.M. Yu, Xu Li, Y.M. Yang, P.L. Li, Luminescence properties of $Ba_2LiB_5O_{10}:Dy^{3+}$ phosphor, Mater. Lett. 65 (2011) 1956–1958.
[7] P. Huang, C Cui, S. Wang, Influence of calcination temperature on luminescent properties of $Sr_3Al_2O_6:Eu^{2+}$, Dy^{3+} phosphors prepared by sol–gel combustion processing, Opt. Mater. 32 (2009) 184–189.
[8] Y.H. Chen, X.R. Cheng, Z.M. Qi, M. Liu, C.S. Shi, Comparison study of the luminescent properties of the white-light long afterglow phosphors: $Ca_xMgSi_2O_{5+x}:Dy^{3+}$ ($x=1,2,3$), J. Lumin. 29 (2009) 531–535.
[9] Sang Do Han, S.P. Khatkar, V.B. Taxak, Gaytri Sharma, Dinesh Kumar, Synthesis luminescence and effect of heat treatment on the properties of Dy^{3+} doped YVO_4 phosphor, Mater. Sci. Eng. B 129 (2006) 126–130.
[10] Adrie J.J. Bos, Pieter Dorenbos, Aurélie Bessière, Bruno Viana, Lanthanide energy levels in YPO_4, Radiat. Meas. 43 (2008) 222–226.
[11] K. Mishra, S.K. Singh, A.K. Singh, S.B. Rai, Optical characteristics and charge transfer band excitation of Dy^{3+} doped Y_2O_3 phosphor, Mater. Res. Bull. 47 (2012) 1339–1344.

[12] P. Huang, F. Yang, C. Cui, L. Wang, X. Lei, Luminescence properties of white-light long-lasting phosphor $Y_2O_2S:Dy^{3+}$, Mg^{2+}, Ti^{4+}, Ceram. Int. 39 (2013) 7193–7197.
[13] Y Murazaki, K Arai, K. Ichinomiya, A new long persistence red phosphor, Jpn. Rare Earth 35 (1) (1999) 41–45.
[14] Y. Tian, B.J. Chen, BN. Tian, R.N. Hua, Concentration-dependent luminescence and energy transfer of flower-like $Y_2(MoO_4)_3:Dy^{3+}$ phosphor, J. Alloys Compd. 509 (2011) 6096–6101.
[15] P.L. Li, Z.C. Zhang, K. Zhang, Z.P. Yang, Z.J. Wang, Q.L. Guo, Effect of charge compensation on emission spectrum of $Ca_2SiO_4:Dy^{3+}$ phosphor, Chin. Opt. Lett. 6 (4) (2008) 274–275.
[16] J. Wan, L.H. Cheng, J.S. Sun, H.Y. Zhong, X.P. Li, Energy transfer and colorimetric properties of Eu^{3+}/Dy^{3+} co-doped $Gd_2(MoO_4)_3$ phosphors, J. Alloys Compd. 496 (2010) 331–334.
[17] B. Liu, C.S. Shi, Z.M. Qi, Potential white-light long-lasting phosphor: Dy^{3+}-doped aluminate, Appl. Phys. Lett. 86 (2005) 191111.
[18] B.F. Lei, H.R. Zhang, W.J. Mai, S. Yue, Y.L. Liu, S.Q. Man, Luminescent properties of orange-emitting long-lasting phosphorescence phosphor $Ca_2SnO_4:Sm^{3+}$, Solid State Sci. 13 (2011) 525–528.
[19] P.F. Ai, W.Y. Li, L.Y. Xiao, Y.D. Li, H.J. Wang, Y.L. Liu, Monodisperse nanospheres of yttrium oxysulfide: synthesis, characterization, and luminescent properties, Ceram. Int. 36 (2010) 2169–2174.
[20] L. Jing, C.K. Chang, D.L. Mao, B. Zhang, A new long persistent blue-emitting $Sr_2ZnSi_2O_7:Eu^{2+}$, Dy^{3+} prepared by sol–gel method, Mater. Lett. 58 (2004) 1825–1829.
[21] P.F. Ai, Y.L. Liu, L.Y. Xiao, H.J. Wang, J.X. Meng, Synthesis of $Y_2O_2S:Eu^{3+}$, Mg^{2+}, Ti^{4+} hollow microspheres via homogeneous precipitation route, Sci. Technol. Adv. Mater. 11 (2010) 035002.
[22] R. Chen, Glow curves with general order kinetics, J. Electrochem. Soc.: Solid Technol. 116 (1969) 1254–1257.
[23] Andrei V. Sidorenko, Adrie J.J. Bos, Pieter Dorenbos, Carel W.E. van Eijk, Andrée Kahn-Harari, Piotr A. Rodnyi, Bruno Viana, Storage effect in $LiRESiO_4:Ce^{3+}$, Sm^{3+}, RE=Y, Lu phosphor, Nucl. Instrum. Methods Phys. Res. A 537 (2005) 81–85.
[24] P.Y. Zhang, Z.L. Hong, H.X. Shen, Z.X. Xu, X.P. Fan, Luminescence characterization of Mg Doped Y2O2S:Ti long afterglow phosphor, J. Rare Earths 24 (2006) 115–118.